Energy & Environmental Science

PAPER

View Article Online
View Journal | View Issue

Cite this: *Energy Environ. Sci.*, 2018, **11**, 1803

The role of the solid electrolyte interphase layer in preventing Li dendrite growth in solid-state batteries†

Bingbin Wu,‡[a] Shanyu Wang,‡[b] Joshua Lochala,[a] David Desrochers,[a] Bo Liu,[c] Wenqing Zhang,[d] Jihui Yang*[b] and Jie Xiao*[ae]

Received 16th February 2018,
Accepted 25th April 2018

DOI: 10.1039/c8ee00540k

rsc.li/ees

Lithium (Li) metal anodes have regained intensive interest in recent years due to the ever-increasing demand for next-generation high energy battery technologies. Li metal, unfortunately, suffers from poor cycling stability and low efficiency as well as from the formation of dangerous Li dendrites, raising safety concerns. Utilizing solid-state electrolytes (SSEs) to prevent Li dendrite growth provides a promising approach to tackle the challenge. However, recent studies indicate that Li dendrites easily form at high current densities, which calls for full investigation of the fundamental mechanisms of Li dendrite formation within SSEs. Herein, the origin and evolution of Li dendrite growth through SSEs have been studied and compared by using $Li_{6.1}Ga_{0.3}La_3Zr_2O_{12}$ (LLZO) and NASICON-type Li_2O–Al_2O_3–P_2O_5–TiO_2–GeO_2 (LATP) pellets as the separators. We discover that a solid electrolyte interphase (SEI)-like interfacial layer between Li and SSE plays a critical role in alleviating the growth of dendritic Li, providing new insights into the interface between SSE and Li metal to enable future all solid-state batteries.

Broader context

The use of lithium (Li) metal anodes in Li-ion batteries has regained intensive research interest because of its capability to significantly boost the energy density of state-of-the-art batteries. For batteries using liquid electrolytes, however, Li continuously reacts with the electrolytes through irreversible reactions, leading to rapid depletion of both the electrolytes and the Li metal, hence resulting in battery failure. Furthermore, the formation of dendritic Li in liquid cells causes severe safety concerns, limiting the wide adoption of rechargeable Li metal-based batteries. Recent studies on solid-state cells using a Li metal anode and a garnet-based solid electrolyte also revealed 'short circuit' phenomena due to the formation of Li dendrites penetrating the solid-state electrolyte. In this work, we discover that an appropriate solid electrolyte interphase (SEI) between a solid electrolyte and the Li metal is required to slow down and eventually terminate the Li dendrite propagation through the phase boundaries of ceramic electrolytes. We further demonstrate that silicon nanoparticle surface filling on a garnet solid electrolyte significantly improves the electrochemical and cycle performance of Li/LLZO/Li cells. The attributes for ideal SEIs are discussed.

Introduction

A steady increase in the demand for high energy batteries has rekindled interest in Li metal anodes, which feature both high gravimetric and high volumetric energy densities.[1] However, Li metal is thermodynamically unstable in liquid electrolytes and continuously consumes the electrolyte without forming a stable SEI.[2,3] In addition, the swelling of Li metal during cycling forms a porous structure which increases the cell impedance and quickly dries up the liquid electrolytes.[4] More importantly, the random formation of detrimental Li dendrites[5] may cause an internal short triggering battery fire/explosion. To address the Li dendrite issue, SSEs have been proposed to physically suppress the growth of Li branches and eliminate the irreversible liquid electrolyte consumption. Based on the Monroe–Newman model, it is expected that SSEs with higher shear moduli, at least twice that of Li metal, can effectively suppress Li dendrites at the interface.[6] Successful synthesis of SSEs, with high ionic conductivities comparable to those of liquid electrolytes, has greatly accelerated the development of all-solid-state batteries.[7,8] Despite the fact that most fully dense inorganic SSEs have shear

[a] *Department of Chemistry and Biochemistry, University of Arkansas, Fayetteville, AR 72701, USA. E-mail: jiexiao@uark.edu*
[b] *Materials Science and Engineering Department, University of Washington, Seattle, WA 98195, USA. E-mail: jihuiy@uw.edu*
[c] *Materials Genome Institute, Shanghai University, Shanghai 200444, China*
[d] *Department of Physics, Southern University of Science and Technology, 1088 Xueyuan Rd., Shenzhen, Guangdong, 518055, China*
[e] *Pacific Northwest National Laboratory, Richland, WA 99252, USA*

† Electronic supplementary information (ESI) available: Fig. S1–S14 and Tables S1 and S2. See DOI: 10.1039/c8ee00540k

‡ These authors contributed equally to this work.

moduli >7 GPa (twice that of Li metal), recent experiments reported 'short circuit' phenomena in garnet-based all solid cells when the current density is increased. The garnet-phase solid electrolyte is stable towards Li metal and the ceramic pellets used in these experiments were sintered and densified at high temperatures.[9] It was further revealed that Li dendrites propagate through a polycrystalline garnet solid electrolyte preferentially along the grain boundaries.[10]

So far, the fundamental principles that govern the origin and evolution of Li dendrite growth along the phase boundaries or defective sites of garnet LLZO are unknown, which hinders the development of practical solid-state batteries or the use of Li metal anodes. Our recent work on the interplay between SEI and Li dendrite growth in liquid cells revealed that, in general, glass-fiber-based separators favor the formation of detrimental Li dendrites in concentrated electrolytes compared with the regular 1 M ones.[11] This is due to the relatively 'thin' and more conductive SEI derived from the concentrated electrolytes, which cannot completely 'stop' the continuous growth of the detrimental Li dendrites. A solid electrolyte can be considered as an extreme case of the 'concentrated' electrolyte that is completely solvent free. It is therefore hypothesized that an appropriate 'SEI' between the solid electrolyte and Li is required to slow down and eventually terminate the Li dendrite propagation through the phase boundaries of ceramic electrolytes. In order to validate this hypothesis, two different electrolytes, LLZO and LATP, have been tested in Li/SSE/Li symmetric cells. The former is stable towards Li metal and is thus essentially 'SEI' free, while the latter is known to react with Li and produces interfacial products in between, forming an inter-layer that mimics the SEI formed in liquid cells. The failure mechanisms of these Li/SSE/Li symmetrical cells containing LLZO and LATP SSEs are studied side-by-side to elucidate the fundamental roles of the SEI layers in the propagation of Li dendrites in solid-state cells. Theoretical simulations have also been integrated in this work to validate the experimental findings.

Experimental section

Materials and characterization

Materials. Square sheets of LATP (EQ-CGCS-LD, thickness × width × length: 0.15 mm × 5 mm × 5 mm) were purchased from the MTI Corporation (USA) and used without any further treatment. Si nanoparticles (polycrystalline silicon, >98%, 30–50 nm, laser synthesized) were purchased from US Research Nanomaterials, Inc. and used without any further treatment. 1 M LiTFSI DME/DOL (1 : 1, by volume) was prepared by dissolving 0.287 g LiTFSI (battery grade, BASF, Germany) into the mixed solvents of 0.5 mL DME (1,2-dimethoxyethane, battery grade, BASF, Germany) and 0.5 mL DOL (1,3-dioxolane, battery grade, BASF) in an argon filled glove box (O_2 < 0.5 ppm, H_2O < 0.5 ppm, MBRAUN, Germany).

$Li_{6.1}Ga_{0.3}La_3Zr_2O_{12}$ (LLZO) preparation. The samples were prepared by a solid-state reaction with subsequent densification by spark plasma sintering (SPS). High purity $LiOH{\cdot}H_2O$ (99.9 5%, Sigma-Aldrich, USA), La_2O_3 (99.99%, Sigma-Aldrich, USA), ZrO_2 (99.9%, Sigma-Aldrich, USA), and Ga_2O_3 (99.99%, Sigma-Aldrich, USA) were used as raw materials. $LiOH{\cdot}H_2O$ was heated at 250 °C for 5 h to get rid of the water, and ZrO_2 and La_2O_3 were also pre-dried at 600 °C for 6 h. Stoichiometric amounts of the powders, according to the nominal composition $Li_{6.1}Ga_{0.3}La_3Zr_2O_{12}$, were mixed by dry ball milling using a ZrO_2 jar and balls (8000M mixer, Spex, USA) for 1 h. An extra 10% Li precursor was added to compensate for the Li losses during the high-temperature synthesis. The mixed powders were cold pressed into pellets with a diameter of 10 mm (450 MPa) and fired at 900–1000 °C for 8–12 h in air on the ZrO_2 plates (placed into Al_2O_3 crucibles and loosely covered) to avoid unintentional Al-doping from the Al_2O_3 crucibles. To avoid contamination by ambient H_2O or CO_2 (Fig. S1 and S2, ESI†),[12,13] the fired LLZO pellets were immediately transferred into a glovebox and pulverized into fine powders inside the glovebox. The pulverized powders were sintered into dense pellets by SPS at ~950–1050 °C under 40 MPa for 5 min and then stored inside the glovebox. The thickness of the pellets was around 690 μm with a diameter of 10 mm. The X-ray diffraction (XRD) pattern of the as prepared LLZO powders can be well identified as LLZO and is consistent with the literature (Fig. S3a and b, ESI†).[14] The fractural surface of the LLZO pellet shows a high compaction with some small voids under an scanning electron microscopy (SEM) (Fig. S3c, ESI†), and the LLZO pellet has an ionic conductivity larger than 1.0 mS cm^{-1} at room temperature (Fig. S3d, ESI†).

Nano-Si filling of the LLZO (Fig. 6a). Both sides of the LLZO were first polished to remove the surface contaminants with a polishing tool (Dremel, USA). A tape with a hole of 5/16 inch (7.94 mm) in diameter was used to cover the top of the LLZO, and subsequently some Si nanoparticles were placed to cover the exposed LLZO, followed by polishing for 1–2 min. The whole process was repeated three times. After finishing one side, the same procedure was carried out for the other.

Material characterization. The phase and purity of the bulk samples were determined by XRD (Bruker D8 Advance X-ray diffraction, Germany) using Cu Kα radiation (λ = 1.5406 Å), and the lattice parameters were refined using the full profile Rietveld method, as implemented in the program TOPAS.[15] The microstructure of the sintered samples' fractural surfaces and morphology of nano-Si particles was examined by a Field Emission SEM with an accelerating voltage of 15 kV (FESEM, FEI Sirion XL30, USA). AC impedance measurements were performed for ionic conductivity tests in the frequency range from 0.01 Hz to 1 MHz with an amplitude of 50 mV using a PARSTAT 4000A Potentiostat (Ametec Scientific Instruments, USA). Prior to the measurements, an Ag paste was sprayed on both sides of the dense pellet and heated in vacuum at 110 °C for 2 h to vaporize the solvent. An optical microscope (ME-520T, AmScope, USA) in a glovebox and a SEM coupled with Energy-dispersive X-ray Spectroscopy (EDS) (FEI Sirion XL30, USA) were used to characterize the SSE separators after cycling. Surface analysis of major elements for LATP and LLZO before and after cycling in the Li/SSE/Li symmetric cells was carried out with X-ray photoelectron spectroscopy

(XPS, PHI VersaProbeIII, USA) and the peaks were fitted using the XPSPEAK 4.1 software. Due to the air exposure (<10 s) during transfer of the samples to the XPS instrument, a surface layer formed blocks the XPS signal (Fig. S4a–c, ESI†), and thus prior to collecting XPS data, Ar^+ ion beam sputtering for 2–3 min was applied to remove the surface contaminates on the cycled SSEs.

Cell assembly and testing

Li/SSE/Li symmetric cells were used to investigate the interfacial properties of LATP and LLZO against Li metal. For the thin and easily fractured LATP square sheets (0.15 mm × 5 mm × 5 mm), Li/LATP/Li symmetric cells were assembled by symmetrically attaching two Li metal chips (3.18 mm in diameter (made with a 2/16 inch round steel hole puncher) and 250 μm in thickness) onto both sides of the LATP and fixing them with tape in the glovebox. Copper foil was used as the current collector for the Li metal (Fig. S5a, ESI†). For the thick LLZO pellets (10 mm in diameter and 690 μm in thickness), custom made module cells[16] were used to assemble the Li/LLZO/Li symmetric cells, and the Li metal chips (4.76 mm in diameter (made with a 3/16 inch round steel hole puncher) and 250 μm in thickness) were used (Fig. S5b, ESI†). The LLZO pellets were polished to remove the hydroxide/carbonate layer prior to assembling the cells. The Li/SSE/Li cells were assembled and cycled at room temperature using a CT2001A battery tester (LANDT, China) in the glovebox. The cells were charged/discharged at a 0.1 mA cm^{-2} current density (4 hours for each charge/discharge cycle). After these cells failed, the cells were disassembled in the glovebox and the SSEs were collected for further characterization. Some cycled SSE pellets were exposed to lab air (20 °C, 40% relative humidity) for 3 days and then washed by a H_2O/ethanol mixture to investigate their surface properties.

Computational method

All calculations were performed within the generalized gradient approximation (GGA) using the Perdew, Burke and Ernzerhof (PBE) exchange–correlation functional;[17] a plane wave basis set and the projector augmented wave (PAW) method[18,19] were used, as implemented in the Vienna Ab initio Simulation Package (VASP).[20,21] The Brillouin zone is sampled by using a 3 × 3 × 2 Monkhorst–Pack[22] grid for $Li_{1.5}Al_{0.5}Ti_{1.5}(PO_4)_3$ (LATP) and a 2 × 2 × 2 one for $Li_{6.25}Ga_{0.25}La_3Zr_2O_{12}$ (LLZO). The energy cutoff for the plane waves was set to 500 eV. The convergence thresholds for self-consistency and forces are 10^{-5} eV and 10^{-2} eV $Å^{-1}$, respectively.

To examine the thermodynamic stability, we calculated the decomposition reaction energy of LATP and LLZO when reacting with metallic lithium through the reduction and decomposition of LATP and LLZO. The decomposition reaction energy was calculated by

$$\Delta E = E(\text{phase equilibria}) - E(\text{solid electrolyte}) - nE(\text{Li})$$

where E(phase equilibria) is the total energy of the phase equilibria, E(solid electrolyte) the total energy of the solid electrolyte, and nLi the change of the amounts of Li from the solid electrolyte composition to the phase equilibria composition during the lithiation reaction. E[Li] is the total energy of metallic lithium in a body-centered-cubic (bcc) unit cell.

The compositions of LLZO and LATP used in the DFT calculations were slightly different from those of the SSE samples to reduce the computational cost. This will not change the overall conclusion of the study.

Results and discussion

Side-by-side comparison of LATP and LLZO

In order to isolate the potential interfacial reactions between SSE and Li, no surface modification was applied to either one of the SSEs before testing. It is known that a surface coating will largely improve the cycling stability[23] (although the current density still needs to be low regardless of the surface coating), but such treatment will contaminate the interfacial reactions. LLZO and LATP were both assembled in Li/SSE/Li symmetrical cells and tested at the same current density of 0.1 mA cm^{-2} as illustrated in Fig. 1. After cycling for about 8 hours, the Li/LLZO/Li cell started to short, indicated by the voltage polarization suddenly dropping to *ca.* 0 V (Fig. 1a).[24] It is noted that during charging, the cell voltage is not zero, suggesting that the Li dendrite growth pathways are different for the two sides of the same LLZO pellet. The surface conditions, *e.g.*, the population of defective sites and the arrangement of voids on the two sides of the LLZO pellet, dictate the Li propagation through the LLZO. The length and diameter of the Li dendrites also vary from nano to micrometers, which leads to resistances of vastly different magnitudes. Accordingly, Li dendrites with various dimensions have different impacts on the cell voltage which does not necessarily become zero all the time; sometimes a voltage fluctuation is also seen, indicative of a cell short (Fig. 1a). The photos of the cycled LLZO clearly display 'dark lines' on the surface, which penetrate

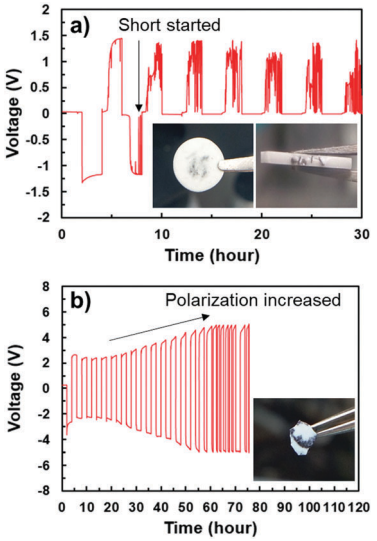

Fig. 1 Cyclic performance of (a) Li/LLZO/Li and (b) Li/LATP/Li symmetric cells at room temperature with a 0.1 mA cm^{-2} current density. Inset: Digital photographs of (a) the surface and cross section of the cycled LLZO and (b) the surface of the cycled LATP (the cross section of the cycled LATP is not shown, as it is too thin to be seen with a digital camera).

throughout the whole pellet (insets of Fig. 1a), consistent with literature reports.[10,25,26] In contrast, the Li/LATP/Li cell fails in a completely different mode. A drastic increase of polarization, instead of a short, terminates the cell after 60 hours (Fig. 1b), suggesting an internal disconnection of the cell. The cycled LATP pellet (inset of Fig. 1b) shows large areas of black deposits on the SSE surface, which are distinctly different from the "narrow" black lines embedded within the LLZO pellet (inset of Fig. 1a).

The optical image of the cycled LLZO (Fig. 2a) only shows scattered black dots on the surface, which are found to be "pits" (Fig. 2b and c) deeply penetrating into the pellet (Fig. 2d) by using SEM and have been reported to be Li dendrites.[8,9,27] We will discuss these later. Interestingly, for the cycled LATP, numerous round dots are visible on the pellet surface (Fig. 2e–g). LATP is known to react with Li,[28] thus these black dots should be the reaction products. Upon closer inspection, these black areas expand above the LATP surface while penetrating into the pellet (Fig. 2h), indicating a localized volume expansion due to the reactions between the Li and the LATP which seem to be self-terminating rather than propagating throughout the entire LATP pellet. These reacted interfacial layers should be ionically conductive, at least in the beginning; otherwise, the Li/SSE/Li cells would not be able to cycle at all.

Interfacial understanding

To further discern the interphases formed between SSE and Li, cycled LLZO and LATP pellets were exposed to air. Cycled LLZO does not display obvious change on the pellet surface (Fig. 3a), except for a few 'fibers' at the 'pits' of the pellet (Fig. 3b). Large amounts of fibers sprout along the cross section of the LLZO pellet with an average diameter of 1–2 μm (Fig. 3c and d). EDS mapping shows that these fibers are highly oxygen-rich (Fig. S6, ESI†) and they can be completely removed after washing the LLZO pellet with a mixture of water and alcohol (Fig. S7, ESI†). Therefore, it is reasonable to assign these fibers in Fig. 3c as lithium hydroxide/carbonate, consistent with the XPS results (Fig. S4c and f, ESI†), which mainly originate from the Li deposits. The occurrence of these 'fibers' suggests that the dendrites formed within the LLZO pellets occur at a greater frequency than captured with SEM due to the nanoscale dimensions of the Li dendrites. Only after having been exposed to air and converted to their hydroxide/carbonate forms with enlarged diameters (*ca.* 2 μm), are these originally nano-sized Li dendrites detectable by SEM. In contrast, the morphologies of the reaction products on the surface (Fig. 3e and f) and the cross section (Fig. 3g and h) of the LATP exhibit minimum change after exposure to air except for some newly formed cracks, most likely due to further reactions with moisture and/or CO_2 in the air. Some of the surfaces are covered by sheet-like products. EDS results indicate that these sheet-like areas have increased Ti and P but decreased Ge content, compared to the rest of the area on the same pellet surface (Fig. S8, ESI†). The additional side reactions between the cycled LATP and air probably generate the Ti- and P-rich byproducts. Exposure to the air does not lead to large changes on the bare LATP (see the cross section of Fig. 2h). The products generated from the reactions between the Li and the LATP do not dissolve in water (Fig. S9, ESI†), indicating that the observed dark reaction products do not contain any Li metal dendrite. XPS analysis also indicates no valence change for the LLZO before and after cycling (Fig. S10, ESI†), demonstrating its superior stability against Li metal. For the cycled LATP, however, new peaks belonging to Ti^{3+} (the peaks of 462.6 eV and 457.2 eV in Fig. 4b) reduced from Ti^{4+} (the peaks of 465.2 eV and 459.4 eV in Fig. 4a), have been detected, while the ratio of Ti^{4+}/Ti^{3+} is estimated to be around 1.7 (Table S1, ESI†).[28] In addition, a small amount of Ge^{2+} is also identified at ~31.1 eV, accounting for *ca.* 8.8% of the total Ge content in the LATP (Fig. 4c and d).[29] These results indicate the reduction of Ti^{4+} and Ge^{4+} during the cycling of the LATP. No valance variation is found for Al^{3+} or P^{5+} (see Fig. S11 for details, ESI†).

Simulation of the interfacial stability

Density functional theory (DFT) calculations of the reaction mechanisms between Li metal and LLZO/LATP were carried out to understand the interactions between the solid electrolytes

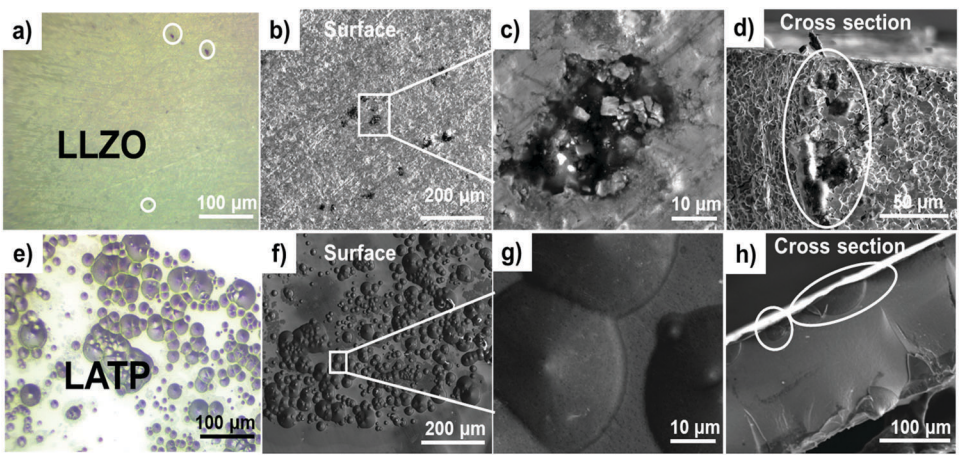

Fig. 2 Morphologies of the surface and cross section of (a–d) the cycled LLZO and (e–h) the cycled LATP shown in Fig. 1. (a and e) Optical images of the surfaces of the cycled LLZO and LATP. (b and f) SEM images of the surfaces of the cycled LLZO and LATP and their enlarged areas (c and g). (d and h) SEM images of the cross sections of the cycled LLZO and LATP.

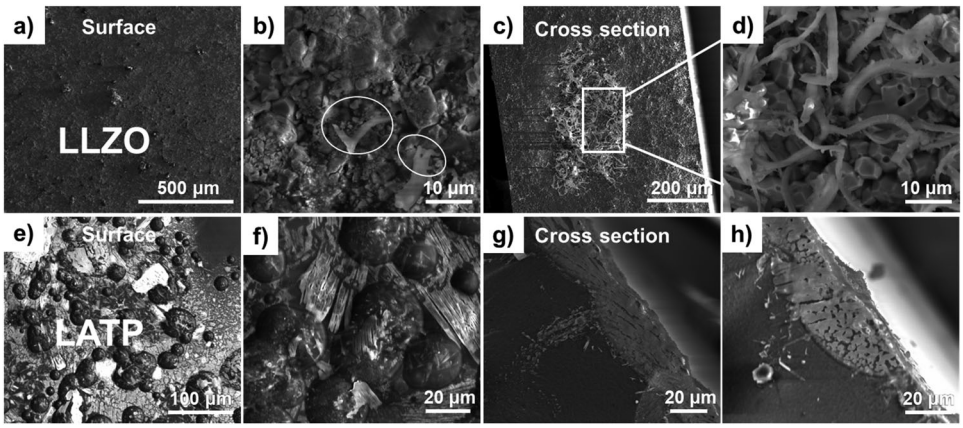

Fig. 3 SEM images of the surfaces and cross sections of (a–d) the cycled LLZO and (e–h) the cycled LATP shown in Fig. 1 after being exposed to the air for 3 days. (a and e) Surface morphologies of the air-treated cycled LLZO and LATP, and their corresponding enlarged areas (b and f). (c and g) Cross sections of the air-treated cycled LLZO and LATP, and their corresponding enlarged areas (d and h).

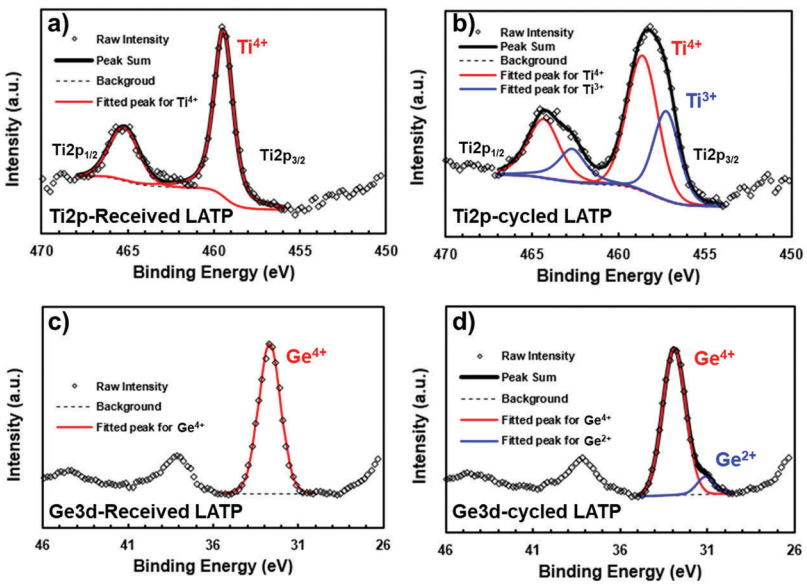

Fig. 4 XPS results of Ti 2p (a and b) and Ge 3d (c and d) of the LATP before and after cycling in the Li/LATP/Li symmetric cell.

and Li metal. For $Li_{6.25}Ga_{0.25}La_3Zr_2O_{12}$, we examined all possible decomposition products. All decomposition phase structures in this work were acquired from the Materials Project database.[30] The possible reaction formulas between LLZO and Li metal are listed in ESI,† and the phase equilibria and Gibbs free energies are summarized in Table S2, ESI.† It is obvious that for all possible cases the Gibbs free energies are positive, indicating that these reactions are thermodynamically unfavorable. These results are well consistent with our experimental observations, which show no chemical or electrochemical reaction between Li and LLZO. For LATP, a representative chemical reaction with Li is

$$6Li_{1.5}Al_{0.5}Ti_{0.83}Ge_{0.67}(PO_4)_3 + 13Li \rightarrow 3AlPO_4 + 6Li_3PO_4 + 5TiPO_4 + 4LiGePO_4, \quad \Delta G = -30.4 \text{ eV}. \qquad (1)$$

The very negative Gibbs free energy ($\Delta G = -30.4$ eV) of this reaction implies that LATP is highly reactive with Li metal at ambient conditions. This reaction is mainly composed of the reduction of Ti^{4+} and Ge^{4+} by Li, as well as the rearrangement and recombination of $[PO_4]^{3-}$ with other cations. It is also well consistent with the XPS data of the cycled LATP, further corroborating the chemical reactivity of Li/LATP by reducing Ti^{4+} and Ge^{4+} on the contact surface. We have also analyzed other possible reaction processes, some of which show negative Gibbs free energies. Nonetheless, sluggish kinetics largely limit or prohibit the occurrence of these reactions. For instance, the reaction accompanied by the reduction of P^{5+} in PO_4^{3-} to P requires the breaking of a strong P–O bond, complex charge transfer, and ion diffusion (O and P) that is slow, and therefore should be kinetically limited. Most importantly, the reaction products are electronic insulators, which should terminate further Li/LATP reactions and the dendritic Li plating through defects and grain boundaries. Meanwhile, the reaction products in eqn (1) are either good ionic conductors ($LiGePO_4$ and Li_3PO_4)

or can be further transformed into ionic conductors ($LiAlPO_5$ or Li_2TiPO_5), ensuring Li-ion transport through the interfacial layer, as observed in our experiments.

Hypothesis validation

From the above observation, although LLZO is stable against Li metal, the non-uniform distribution of the electrical field on Li/LLZO surfaces still promotes the formation of dendritic Li that grows along the defects and phase boundaries vertical to the LLZO surface. A higher current density induces more inhomogeneous Li depositions, *i.e.*, dendrites shorting the solid cells (Fig. 1a), which explains why the current density cannot exceed 0.5 mA cm^{-2} in order to reduce the chance of a cell short.[9] For LATP that directly contacts and reacts with Li (Fig. S12, ESI†), the interfacial reaction products can also be considered as an SEI between the Li and the LATP, similar to those formed in liquid cells. Of note, in solid and liquid cells, the SEI is on the surfaces of the SSE and the Li metal, respectively. The function of the SEI is nevertheless similar, *i.e.*, to conduct Li^+ ions across this interphase. Imagining that dendritic Li forms and touches the LATP, it will react with the LATP and convert itself in building the 'SEI'. Once the SEI is formed, due to its electronic insulating nature, the continuous growth of Li dendrites along this direction is prevented. The ionically conductive SEI formed on the LATP surface allows the flow of Li^+ ions; hence, the cell displays a certain cyclability. As the reactions proceed in all directions, the 'thickened' SEI cannot transfer Li^+ ions promptly and this increases the cell impedance, consistent with the large polarization observed after only a few cycles that eventually terminates the cell. Many cracks have also been identified on the cycled LATP pellet. The cracks perfectly connect all the dark spots (Fig. S13, ESI†), indicating that the local stress near the reaction products between the LATP and the Li leads to the further 'breakdown' of the LATP pellet. Even for those cracks within the pellet, no Li dendrite is found, which will be discussed later. These findings seem to suggest that if the surface coating layer on ceramic electrolytes forms an ionically conductive interphase by directly reacting with Li and this interfacial layer does not grow further, Li dendrite formation may be significantly reduced, leading to stable cell cycling.

A convenient way to validate the necessity of forming an SEI between the solid electrolyte and the Li metal is to add a trace amount of liquid electrolyte to the surface of the solid electrolyte. The liquid electrolyte can quickly react with Li dendrites to form an SEI, thus preventing them from growing through the solid electrolyte pellet. One drop (10 μL) of 1 M LiTFSI-DOL/DME was added to both sides of the LLZO pellet when assembling the Li/LLZO/Li symmetric cell. The motivation for using 1 M LiTFSI-DOL/DME is that the formed SEI has a relatively high resistance compared to other regular electrolytes,[11] thereby the growth of Li tips can be 'slowed down'. The reversible cycling of the Li/SSE/Li cell is greatly improved to 30 hours (Fig. 5) after adding only 10 μL of liquid electrolyte, strongly supporting our hypothesis that an 'SEI' is critically needed to cover the Li surface to mitigate and eventually eliminate the fast propagation of

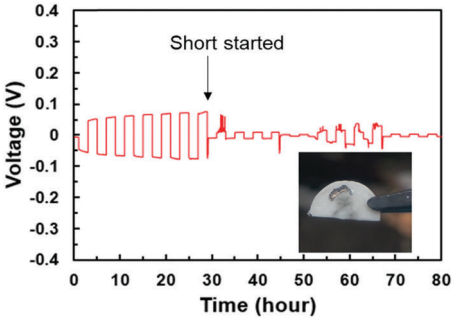

Fig. 5 Cyclic performance of the Li/LLZO/Li symmetric cell at room temperature with a one-drop (10 μL) liquid electrolyte on both of the two surfaces of the LLZO between the SSE and the Li metal. Liquid electrolyte: 1 M LiTFSI-DOL/DME, current density: 0.1 mA cm^{-2}. Inset: Digital image of the cycled LLZO pellet harvested from the failed cell.

dendritic Li. After 30 hours reversible stripping/deposition of Li, the cell was eventually shorted (see dark lines in Fig. 5 (inset)). The depletion of the small amount of liquid electrolyte upon cycling led to the reformation of detrimental Li dendrites, which ultimately shorted the cell. In other words, the improvement in the cycling of the liquid electrolyte containing Li/LLZO/Li cell is due to the formation of a 'protective' SEI layer derived from the liquid electrolyte on Li metal. A recent publication reported a 'sandwiching' gel electrolyte between a garnet electrolyte and Li metal that greatly extended the cell cycling at high rates.[31] Considering the fact that the gel electrolyte used is actually polymers swelled by absorbing liquid electrolyte within the polymeric framework, the underlying enabling mechanism of this gel electrolyte is likely the same as the liquid electrolyte added to our cell shown in Fig. 5, *i.e.*, the SEI derived from the gel electrolyte facilitates the 'healthy' cycling of the Li metal anode. When adding liquids, not only is the solid cell resistance reduced, but also the cell short caused by Li dendrites is also significantly alleviated. The former has been commonly used to explain the benefits of adding liquid electrolytes while the latter is seldom recognized or mentioned. As long as the electrolyte is not depleted, the dendritic Li exposed to the liquid electrolyte will be consumed to form an ionically conductive SEI at the interfacial Li/LLZO sites. However, once the liquid electrolyte in the voids or defects dries up, the ability to 'convert' Li dendrites to an SEI disappears. Therefore, the cell short comes back after extended yet still limited cycling in Fig. 5. Note that only a trace amount of liquid electrolyte has been added, which mostly resides within the pores of the LLZO pellet and functions in forming an SEI when Li dendrites come into contact. If the cell is flooded by the electrolyte, due to the different nucleation/growth pathways of Li in liquid *vs.* solid electrolytes, the morphology of the deposited Li will become different and is expected to be affected by the components of the liquid electrolytes. Penetrated Li dendrites (Fig. 2d) may not even be easily observed if too much liquid electrolyte is used.[11]

From the above discussion, an ideal SEI reactant within solid-state cells should possess at least two attributes: (1) the ability to chemically or electrochemically react with Li metal and derive an ionically conductive phase to ensure continuous

Li^+ flow, and (2) the ability to form an ionic conductive interface which is reversible during repeated cycling so that a 'protective' SEI will form repeatedly during cycling. To further substantiate the hypothesis on the critical role of the SEI layer between the Li and the solid electrolyte, silicon (Si) nanoparticles (Fig. 6b) were filled into the LLZO surface structures (Fig. 6c) through a simple and facile 'polishing' process without any further treatment (Fig. 6a). The polishing process helps the Si nanoparticles to reside preferentially in the pores/phase boundary valleys on the LLZO pellet (Fig. 6d–g and Fig. S14, ESI†). When dendritic Li forms and comes into contact with nano-Si at these defective sites, it reacts with part of the Si nanoparticles and converts them into Li–Si alloys, which effectively 'terminates' the further growth of metallic Li dendrites. More importantly, the electrochemical reactions between the Li and the Si are reversible.[32] That is, during the discharge process when the Li is being stripped to the cathode side, the as-formed Li–Si 'returns' the Li source back. Therefore, the Si-filled interfaces between the Li and the LLZO are essentially reversible. Fig. 6e displays the cycling performance of the Li/LLZO/Li symmetric cell using the similar LLZO separator membrane as in Fig. 1a and 5 except that Si nanoparticles have been filled into the surface structures of the membrane through the 'polishing' process (see Experiment section for details). Surprisingly, not only the overpotential for Li deposition/stripping is significantly reduced to less than 50 mV, but also an extremely stable cycling has been achieved for more than 220 hours. The significantly improved electrochemical behavior of LLZO and its interface with Li metal strongly support our hypothesis on the importance of introducing a reversible SEI layer (derived from the Li/Si reaction in this case) between the Li and the SSE. Notably, a uniform Si coating layer on LLZO has been recently reported to improve the wetting between Li and LLZO, so the Li/LLZO interfacial resistance can be largely decreased.[23] However, the purpose of 'filling' Si particles in this work is quite different. The Si filling layer is not uniform on the LLZO since only a high-speed 'brush' was used to decorate nano-Si on the LLZO pellet within a few minutes. No further heat treatment *etc.* was carried out either. Nano-Si here is mainly used to prevent the cell shorting caused by the Li dendrites in our work. A current density of 0.1 mA cm^{-2} has been used to induce Li dendrite formation in this work. At lower rates, given sufficient time of deposition, the growth of dendritic Li through the phase boundaries of the SSE may still occur. Therefore, SEI layers are always needed in all solid-state cells working at different rates. Operando characterization will be conducted in the future to monitor the dynamic interactions between the Li dendrites and the nano-Si fillers within the electrolyte pellets. It is worthwhile pointing out that Coulombic efficiency (CE) is another important parameter to evaluate the electrolyte, since a low CE corresponds to a fast capacity degradation. Although this work mainly focuses on the dendrite-caused cell short, in the future, CE measurements of a solid-state electrolyte in Li metal cells consisting of a standard cathode and a Li metal anode are necessary to fully understand the stability and durability of solid-state electrolytes.

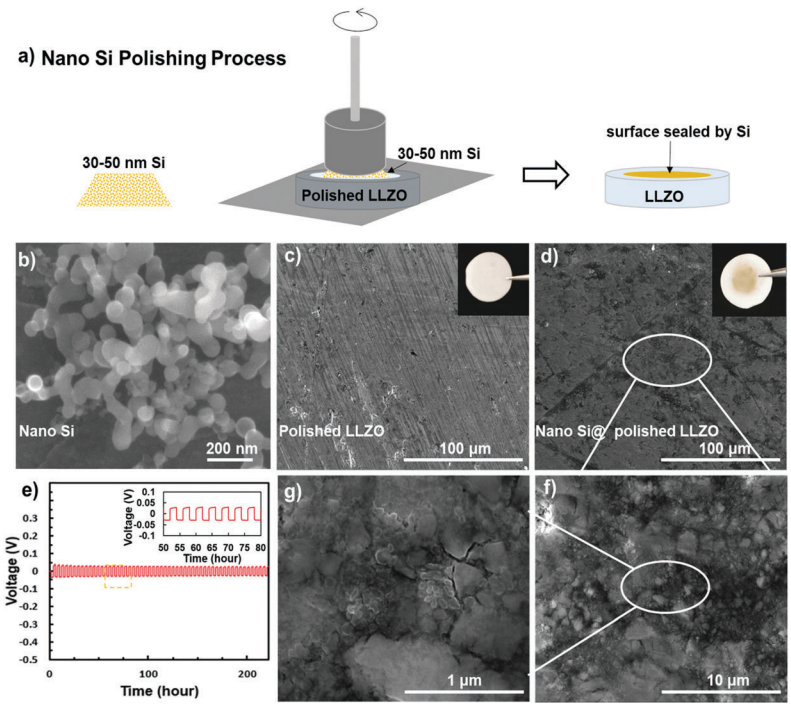

Fig. 6 (a) Schematic diagram of the nano Si polishing process of the LLZO and SEM images of (b) the nano-Si, (c) the surface of the polished LLZO (inset: digital image of the polished LLZO pellet), (d) the surface of the nano Si polished LLZO (inset: digital image of the nano-Si polished LLZO pellet) and enlarged images (f and g). (e) Cyclic performance of the Li/SSE/Li symmetric cell at room temperature with nano-Si polished LLZO as the SSE (inset: enlarged cycles between 50 and 80 hours), current density: 0.1 mA cm^{-2}.

Conclusions

Different cell shorting mechanisms have been observed when using garnet-type LLZO and NASICON-type LATP as the separators in solid-state cells. While the LLZO is stable against Li metal, dendritic Li still forms along the grain boundaries and the defective sites of the LLZO pellet. In contrast, the reactions between the LATP and the Li effectively terminate the continuous Li dendrite propagation; the reaction region expands and eventually blocks Li^+ diffusion, and the cell terminates by substantially increased cell impedance. Post mortem analysis of the cycled LLZO and LATP pellets along with DFT simulation further confirms the stable interface between the LLZO and the Li, while Ti^{4+} and Ge^{4+} in LATP are partially reduced during the reactions with Li and 'SEI'-like layers are formed to prevent further Li dendrite growth. Our study demonstrates that an interfacial SEI layer formed *in situ* between Li and solid electrolytes is crucial to impede continuous Li dendrite growth through the electrolyte phase boundaries. In order to substantiate the roles of the SEI layers, liquid electrolyte or Si nanoparticles were used to fill the surface micro-pores of the LLZO pellets, both of which effectively extend the stable cycling of solid cells. Most importantly, the reversible SEI formed by using Si nanoparticles sheds new light on the significance of rational modifications of the interfacial properties between solid electrolytes and Li in eliminating Li dendrite formation to accelerate the development of solid-state batteries.

Conflicts of interest

There are no conflicts to declare.

Acknowledgements

The authors acknowledge support from the National Science Foundation (NSF) under Grant No. CBET-1748279. JX also thanks the support from Arkansas Research Alliance. SW and JY acknowledge the support from Inamori Foundation. BL and WZ acknowledge the financial support of The National Key Research and Development Program of China (2017YFB0701600) and Program of Shanghai Subject Chief Scientist (16XD1401100).

References

1 D. Lin, Y. Liu and Y. Cui, *Nat. Nanotechnol.*, 2017, **12**, 194.
2 W. Xu, J. Wang, F. Ding, X. Chen, E. Nasybulin, Y. Zhang and J.-G. Zhang, *Energy Environ. Sci.*, 2014, **7**, 513.
3 X. B. Cheng, R. Zhang, C. Z. Zhao, F. Wei, J. G. Zhang and Q. Zhang, *Adv. Sci.*, 2016, **3**, 1500213.
4 D. Lu, J. Tao, P. Yan, W. A. Henderson, Q. Li, Y. Shao, M. L. Helm, O. Borodin, G. L. Graff and B. Polzin, *Nano Lett.*, 2017, **17**, 1602.
5 R. Chianelli, *J. Cryst. Growth*, 1976, **34**, 239.
6 C. Monroe and J. Newman, *J. Electrochem. Soc.*, 2005, **152**, A396.
7 N. Kamaya, K. Homma, Y. Yamakawa, M. Hirayama, R. Kanno, M. Yonemura, T. Kamiyama, Y. Kato, S. Hama and K. Kawamoto, *Nat. Mater.*, 2011, **10**, 682.
8 X. Han, Y. Gong, K. K. Fu, X. He, G. T. Hitz, J. Dai, A. Pearse, B. Liu, H. Wang and G. Rubloff, *Nat. Mater.*, 2017, **16**, 572.
9 R. Sudo, Y. Nakata, K. Ishiguro, M. Matsui, A. Hirano, Y. Takeda, O. Yamamoto and N. Imanishi, *Solid State Ionics*, 2014, **262**, 151.
10 E. J. Cheng, A. Sharafi and J. Sakamoto, *Electrochim. Acta*, 2017, **223**, 85.
11 B. Wu, J. Lochala, T. Taverne and J. Xiao, *Nano Energy*, 2017, **40**, 34.
12 C. Ma, E. Rangasamy, C. Liang, J. Sakamoto, K. L. More and M. Chi, *Angew. Chem.*, 2015, **127**, 131.
13 L. Cheng, J. S. Park, H. Hou, V. Zorba, G. Chen, T. Richardson, J. Cabana, R. Russo and M. Doeff, *J. Mater. Chem. A*, 2014, **2**, 172.
14 S. Afyon, F. Krumeich and J. L. Rupp, *J. Mater. Chem. A*, 2015, **3**, 18636.
15 A. Bruker, Bruker AXS, Karlsruhe, Germany, 2009.
16 X. Yao, D. Liu, C. Wang, P. Long, G. Peng, Y.-S. Hu, H. Li, L. Chen and X. Xu, *Nano Lett.*, 2016, **16**, 7148.
17 J. P. Perdew, K. Burke and M. Ernzerhof, *Phys. Rev. Lett.*, 1996, **77**, 3865.
18 P. E. Blöchl, *Phys. Rev. B: Condens. Matter Mater. Phys.*, 1994, **50**, 17953.
19 G. Kresse and D. Joubert, *Phys. Rev. B: Condens. Matter Mater. Phys.*, 1999, **59**, 1758.
20 G. Kresse and J. Hafner, *Phys. Rev. B: Condens. Matter Mater. Phys.*, 1993, **47**, 558.
21 G. Kresse and J. Furthmüller, *Phys. Rev. B: Condens. Matter Mater. Phys.*, 1996, **54**, 11169.
22 H. J. Monkhorst and J. D. Pack, *Phys. Rev. B: Solid State*, 1976, **13**, 5188.
23 W. Luo, Y. Gong, Y. Zhu, K. K. Fu, J. Dai, S. D. Lacey, C. Wang, B. Liu, X. Han and Y. Mo, *J. Am. Chem. Soc.*, 2016, **138**, 12258.
24 B. Xu, W. Li, H. Duan, H. Wang, Y. Guo, H. Li and H. Liu, *J. Power Sources*, 2017, **354**, 68.
25 A. Sharafi, H. M. Meyer, J. Nanda, J. Wolfenstine and J. Sakamoto, *J. Power Sources*, 2016, **302**, 135.
26 Y. Kim, A. Yoo, R. Schmidt, A. Sharafi, H. Lee, J. Wolfenstine and J. Sakamoto, *Front. Energy Res.*, 2016, **4**, 20.
27 Y. Ren, Y. Shen, Y. Lin and C.-W. Nan, *Electrochem. Commun.*, 2015, **57**, 27.
28 P. Hartmann, T. Leichtweiss, M. R. Busche, M. Schneider, M. Reich, J. Sann, P. Adelhelm and J. R. Janek, *J. Phys. Chem. C*, 2013, **117**, 21064.
29 S. Manna, N. Prtljaga, S. Das, N. Daldosso, S. Ray and L. Pavesi, *Nanotechnology*, 2012, **23**, 065702.
30 A. Jain, S. P. Ong, G. Hautier, W. Chen, W. D. Richards, S. Dacek, S. Cholia, D. Gunter, D. Skinner and G. Ceder, *APL Mater.*, 2013, **1**, 011002.
31 B. Liu, Y. Gong, K. Fu, X. Han, Y. Yao, G. Pastel, C. Yang, H. Xie, E. D. Wachsman and L. Hu, *ACS Appl. Mater. Interfaces*, 2017, **9**, 18809.
32 J. Graetz, C. Ahn, R. Yazami and B. Fultz, *Electrochem. Solid-State Lett.*, 2003, **6**, A194.

